*Inorg. Chem.* **2006**, *45*, 917−922


# Design of a New Family of Inorganic Compounds $Ae_2F_2SnX_3$ (Ae = Sr, Ba; X = S, Se) Using Rock Salt and Fluorite 2D Building Blocks

**Houria Kabbour, Laurent Cario,* Michel Danot, and Alain Meerschaut**

*Institut des Matériaux Jean Rouxel, UMR 6502 CNRS - Université de Nantes, 2 rue de la Houssinière,*
*44322 Nantes Cedex 1, France*

Received September 16, 2005

We could predict the structure of a new family of compounds $Ae_2F_2SnX_3$ (Ae = Sr, Ba; X = S, Se) from the stacking of known 2D building blocks of the rock salt and fluorite types. With a high-temperature ceramic method we have then succeeded to synthesize the four compounds $Ba_2F_2SnS_3$, $Ba_2F_2SnSe_3$, $Sr_2F_2SnS_3$, and $Sr_2F_2SnSe_3$. The structure refinements from X-ray powder diffraction patterns have confirmed the structure predictions and showed their good accuracy. The structure of the four compounds results from the alternated stacking of fluorite $[Ae_2F_2]$ (Ae = Sr, Ba) and distorted rock salt $[SnX_3]$ (X = S, Se) 2D building blocks. As shown by band structure calculations, these blocks behave as a charge reservoir and a charge acceptor, respectively. $Sr_2F_2SnS_3$ and $Ba_2F_2SnS_3$ are transparent with optical gaps of 3.06 and 3.21 eV, respectively. However, an attempt to obtain a transparent conductor by substituting Ba per La in $Ba_2F_2SnS_3$ was unsuccessful.

## Introduction

As a reliable ab initio theory for crystal structure is still lacking, the rational design of new compounds remains a major challenge in solid-state sciences. However, the past 10 years have seen the development of the concept of crystal engineering that transposes the supramolecular chemistry tools (secondary building units (SBU), self-assembly) to the design and synthesis of new hybrid compounds. This concept was particularly successful to create new open framework compounds with the discovery of several families of metal oxide framework compounds.[1−3] In this case the prediction of the structure (inorganic−organic framework) is simplified through the constraints imposed by the assembly of the inorganic SBU by the organic link. New computational methods using a minimal a priori knowledge were used to predict these types of structures and help their structure resolutions from an X-ray powder pattern.[3,4]

In contrast with hybrid compounds, the crystal engineering of inorganic compounds that do not contain an organic part remains an almost unexplored field. Recently, we have shown that we could predict the structures and the compositions of some new pure inorganic compounds by stacking known 2D building blocks of distinct chemical natures.[5−7] This paper reports on the structure prediction of a new family of compounds $Ae_2F_2SnX_3$ (Ae = Sr, Ba; X = S, Se) considering the stacking of tetragonal fluorite $[Ae_2F_2]$ and NaCl $[SnX_3]$ 2D building blocks. Quantum calculation methods were used to optimize the crystallographic structure and calculate the band structures of $Ba_2F_2SnSe_3$. But this paper aims mainly to present the synthesis and the characterization of the target compounds (chemical analysis, structure refinement from X-ray powder diffraction pattern, and Mössbauer study) and to compare the experimental results with the prediction.

## Experimental Section

All compounds $Ba_2F_2SnS_3$, $Ba_2F_2SnSe_3$, $Sr_2F_2SnS_3$, and $Sr_2F_2SnSe_3$ were synthesized using a high-temperature ceramic method.

* To whom correspondence should be addressed. E-mail: Laurent.Cario@cnrs-imn.fr. Phone: 00 33 (0)2 40 37 39 48.

(1) Yaghi, O. M.; O'Keefe, M.; Ockwig, N. W.; Chae, H. K.; Eddaoudi, M.; Kim, J. *Nature* **2003**, *423*, 705−714.
(2) Eddaoudi, M.; Moler, D. B.; Li, H.; Chen, B.; Reineke, T. M.; O'Keefe, M.; Yaghi, O. M. *Acc. Chem. Res.* **2001**, *34*, 319−330.
(3) Ferey, G.; Mellot-Draznieks, C.; Serre, C.; Millange, F. *Acc. Chem. Res.* **2005**, *38*, 217−225.
(4) Mellot-Draznieks, C.; Girard, S.; Ferey, G.; Schön, J. C.; Cancaveric, Z.; Jansen, M. *Chem. Eur. J.* **2002**, *8*, 4103−4113.
(5) Cario, L.; Kabbour, H.; Meerschaut, A. *Chem. Mater.* **2005**, *17*, 234−236.
(6) Kabbour, H.; Cario, L.; Boucher, F. *J. Mater. Chem.* **2005**, *15*, 3525−3531.
(7) Cario, L.; Lafond, A.; Morvan, T.; Kabbour, H.; Deudon, C.; André, G.; Palvadeau, P. *Solid State Sci.* **2005**, *7*, 936−944.

10.1021/ic051592v CCC: $33.50 
Published on Web 12/14/2005

A stoichiometric proportion of $AeF_2$ ($BaF_2$ or $SrF_2$), AeS (BaS or SrS), SnX (SnS or SnSe), and sulfur or selenide element was weighted and ground in an argon glovebox. This mixture was subsequently pressed into pellets and sealed under vacuum in a silica tube. The tube was then heated to 700 °C (at 50 °C/h) for 12 h. For the mixtures containing selenide element, a first step at 220 °C for 12 h was applied before heating at 700 °C, followed by regrinding and annealing at the same temperature.

The X-ray diffraction analyses of all compounds were performed on a D5000 diffractometer using the Cu K$\alpha$ radiations. The data collection was performed at room temperature in the 10−110° 2$\theta$ range with an acquisition time of 12 h. The cell parameters and the crystal structure refinements were performed by the Rietveld method using the programs FullProf[8] and WinPlotr.[9] The background was fitted by a linear interpolation between selected points. The pseudo-Voigt function was used as the peak-shape model in all the refinements. The March-Dollase model for preferred orientation ((010) direction) was used for the refinement of $Sr_2F_2SnSe_3$ and $Sr_2F_2SnS_3$ (refined values 0.9358 and 0.9608, respectively).

The chemical analysis of all compounds was performed on powder samples using an electron microscope equipped with an additional EDX apparatus (energy dispersive analysis of X-rays). The presence of fluorine was confirmed for all compounds but this element could not be quantified due to experimental limitations.

$^{119}$Sn Mössbauer spectra have been recorded using a conventional constant acceleration spectrometer equipped with a ~5 mCi $Ca^{119m}SnO_3$ source. Low-temperature measurements were performed down to 78 K using an Oxford Instruments cryostat (±0.5 K). The spectra were refined according to standard computer techniques. The isomer shift reference is $CaSnO_3$ at room temperature.

Reflectance measurements have been performed using a Varian Cary 5G Spectrometer equipped with a praying mantis.

## Theoretical Calculations

The cell and atomic position parameters of $Ba_2F_2SnSe_3$ were optimized using VASP.[10] The calculations were performed with the Generalized Gradient Approximations (GGA) using the Perdew−Wang 91[11] functional and PAW pseudopotentials.[12] The cutoff energy was 400 eV with a 3 × 1 × 3 Monkhorst-Pack[13] *k*-point mesh. The geometry convergence criterion chosen were the forces with $|F\text{-max}| = 0.03$ eV/Å.

Band structure calculations of $Ba_2F_2SnSe_3$ were performed with the FLAPW method as implemented in the program WIEN2K.[14] We used the generalized gradient approximation of Perdew-Wang 91. The muffin-tin radii are 1.4817, 1.0584, 1.2700, and 1.1642 Å for Ba, F, Sn, and Se, respectively. The cutoff basis set was defined using an $R\text{min}.K\text{max} = 8$. Convergence of the total energy with respect to the *k*-points sampling has been checked and 100 *k*-points were used (9 irreducible).

**Table 1.** Atomic Positions Obtained for the Optimized Hypothetical Structure of $Ba_2F_2SnSe_3$

| atom | site | x | y | z |
|---|---|---|---|---|
| Ba | 8d | 0.7555 | 0.0735 | 0.5048 |
| Sn | 4c | 0.1441 | 1/4 | 0.5888 |
| Se1 | 4c | −0.2586 | 1/4 | 0.5165 |
| Se2 | 8d | 0.2613 | 0.1343 | 0.4848 |
| F | 8d | 0.4984 | 0.0011 | 0.2546 |

**Table 2.** Experimental Atomic Percentages Obtained by Chemical Analysis (EDX) Performed for $Ba_2F_2SnS_3$, $Ba_2F_2SnSe_3$, $Sr_2F_2SnSe_3$, and $Sr_2F_2SnS_3$

| element | theoretical | $Ba_2F_2SnSe_3$ | $Sr_2F_2SnSe_3$ | $Ba_2F_2SnS_3$ | $Sr_2F_2SnS_3$ |
|---|---|---|---|---|---|
| Ae (%) | 33.3 | 35.0 | 35.1 | 33.7 | 32.9 |
| Sn (%) | 16.7 | 17.1 | 16.7 | 15.8 | 16.4 |
| X (%) | 50 | 47.9 | 48.1 | 50.5 | 50.7 |

## Results and Discussion

We have first predicted the structures of $Ba_2F_2SnS_3$, $Ba_2F_2SnSe_3$, $Sr_2F_2SnS_3$, and $Sr_2F_2SnSe_3$ using simple electronic or geometric considerations and literature data. BaFCl[15] presents an electron donor [$Ba_2F_2$] fluorite 2D building blocks. On the other hand, the electron acceptor 2D building block [$SnS_3$] exists in $La_2O_2SnS_3$ and exhibits a distorted NaCl structure.[16] By stacking alternatively the fluorite and NaCl 2D building blocks, we could predict that $Ba_2F_2SnS_3$, $Ba_2F_2SnSe_3$, $Sr_2F_2SnS_3$, and $Sr_2F_2SnSe_3$ would be isostructural with $La_2O_2SnS_3$. To improve this prediction, we optimized the handmade structure of $Ba_2F_2SnSe_3$ using the program VASP that allows relaxing both the cell and atomic parameters. This calculation converged with the predicted structure of $Ba_2F_2SnSe_3$ and Table 1 gives the cell and atomic position parameters for the optimized structure (space group *Pnma*).

We have then tried to synthesize the four compounds $Ba_2F_2SnS_3$, $Ba_2F_2SnSe_3$, $Sr_2F_2SnS_3$, and $Sr_2F_2SnSe_3$ using a high-temperature ceramic method. The reaction products for $Ba_2F_2SnS_3$ (white powder) or for $Ba_2F_2SnSe_3$ (green powder) and $Sr_2F_2SnSe_3$ (orange powder) appeared to be homogeneous. For $Sr_2F_2SnS_3$ we obtained an inhomogeneous sample and we could observe the presence of orange crystals of $SnS_2$. The powder diagrams obtained for $Ba_2F_2SnS_3$, $Ba_2F_2SnSe_3$, and $Sr_2F_2SnSe_3$ gave no hint to the formation of any known binary or ternary compounds. For $Sr_2F_2SnS_3$ we could detect the presence of some impurities, namely, $SrF_2$ (6%) and $SnS_2$ (2%). Chemical analysis revealed the atomic percentages for the Ba, Sn, and S or Se elements (at. %) that are given Table 2. These values compare reasonably well with the theoretical values Ae (Ba or Sr) 33.3%, Sn 16.7%, and X (S or Se) 50% expected for the composition $Ae_2F_2SnX_3$ without considering the fluorine element. Both these analyses and the comparison of the experimental powder diagrams with the simulated powder diagrams obtained thanks to the structure predictions confirmed the formation of the quaternary compounds with the expected structure.

The X-ray powder patterns of the pure sample of $Ba_2F_2SnS_3$, $Ba_2F_2SnSe_3$, and $Sr_2F_2SnSe_3$ were then refined using

(8) Rodríguez-Carvajal, J. FullProf, http://www-llb.cea.fr/fullweb/fp2k/fp2k.htm, 2001.
(9) Roisnel, T.; Rodriguez-Carvajal, J. *Mater. Sci. Forum* **2001**, *378−381*, 118−123.
(10) Kresse, G.; Furthmüller, J. Vienna Ab-initio Simulation Package (VASP), http://cms.mpi.univie.ac.at/vasp/vasp/vasp, 2004.
(11) Perdew, J. P.; Wang, Y. *Phys. Rev. B* **1992**, *45*, 13244.
(12) Kresse, G.; Joubert, D. *Phys. Rev. B* **1999**, *59*, 1758.
(13) Monkhorst, H. J.; Pack, J. D. *Phys. Rev. B* **1976**, *13*, 5188.
(14) Blaha, P.; Schwarz, K.; Madsen, G. K. H.; Kvasnicka, D.; Luitz, J. wien2k: An Augmented Plane-Wave + Local Orbitals Program For Calculating Crystal Properties, http://www.wien2k.at/, 2001.
(15) Sauvage, M. *Acta Crystallogr. B* **1974**, *30*, 2786−2787.
(16) Bénazeth, S.; Guittard, M.; Laruelle, P. *Acta Crystallogr.* **1985**, *C41*, 649−651.

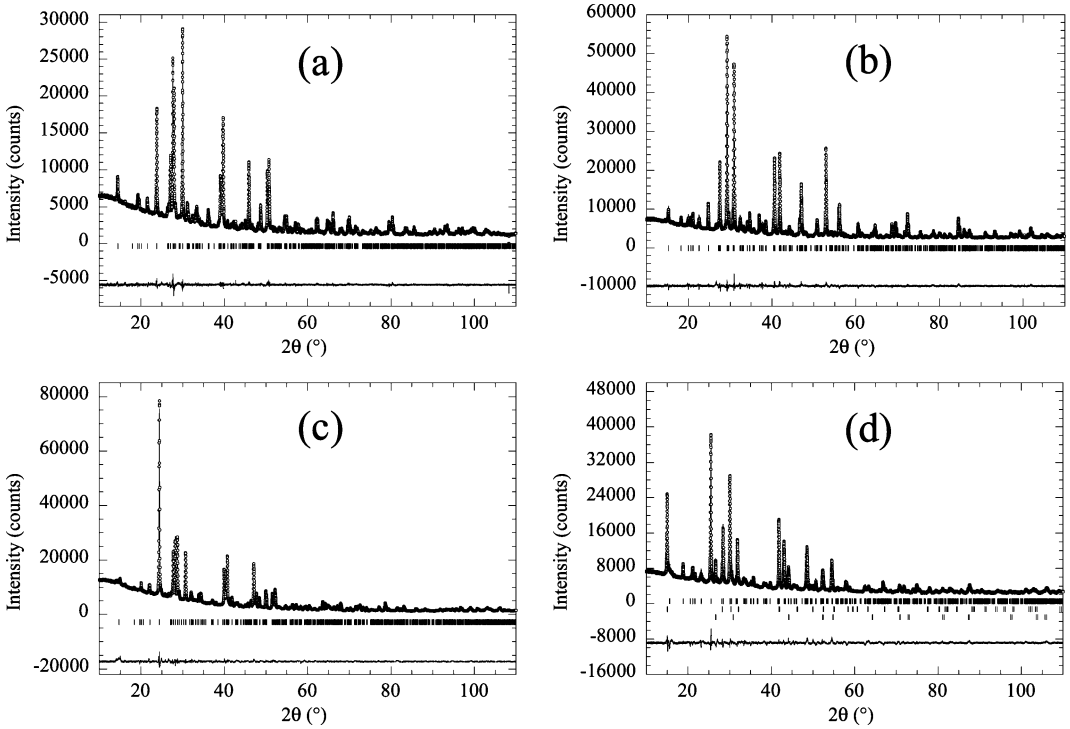


**Figure 1.** Observed X-ray diffraction pattern recorded for $Ba_2F_2SnSe_3$ (a), $Sr_2F_2SnSe_3$ (b), $Ba_2F_2SnS_3$ (c), and $Sr_2F_2SnS_3$ (d) (open circle). The black line represents the calculated intensities by the Rietveld method. The bottom curve is the difference between experimental and calculated intensities.

**Table 3.** Data and Structure Refinement (Space Group *Pnma*) of $Ba_2F_2SnS_3$, $Ba_2F_2SnSe_3$, $Sr_2F_2SnSe_3$, and $Sr_2F_2SnS_3$

| compound | $Ba_2F_2SnSe_3$ | $Sr_2F_2SnSe_3$ | $Ba_2F_2SnS_3$ | $Sr_2F_2SnS_3$ |
|---|---|---|---|---|
| *a* (Å) | 6.3844(1) | 6.1078(4) | 6.2037(4) | 5.9365(9) |
| *b* (Å) | 19.7579(5) | 19.453(7) | 19.2950(11) | 18.842(2) |
| *c* (Å) | 6.4492(1) | 6.1051(5) | 6.3236(1) | 5.9490(9) |
| *V* (Å$^3$) | 813.53(3) | 725.39(8) | 756.91(7) | 665.4(2) |
| *R*-Bragg (%) | 3.63 | 5.25 | 5.34 | 7.61 |
| Rwp[a] (%) | 8.04 | 10.25 | 11.96 | 15.66 |
| Rp[a] (%) | 9.45 | 12.44 | 12.59 | 19.20 |
| Rexp[a] (%) | 5.74 | 4.75 | 4.32 | 5.76 |
| $\chi^2$ | 2.08 | 4.92 | 8.13 | 7.75 |

[a] Corrected for background.

the Rietveld method. Using a multiple-phases procedure that takes into account all impurities, we could also perform a Rietveld refinement for the impure sample of $Sr_2F_2SnS_3$. Starting from the predicted structures of $Ba_2F_2SnS_3$, $Ba_2F_2SnSe_3$, $Sr_2F_2SnS_3$, or $Sr_2F_2SnSe_3$, all refinements converged to satisfying reliability factors (see Table 3). Figure 1a−d shows the experimental powder patterns recorded for all compounds and the best fit we have obtained with FullProf. Refinement results, cell parameters, atomic position parameters, and isotropic displacement parameters are given in Table 4.

The structure of the four compounds $Ae_2F_2SnX_3$ (Ae = Sr, Ba; X = S, Se) is shown in Figure 2. As expected the structure results from the alternated stacking of fluorite type $[Ba_2F_2]$ 2D building blocks and $[SnX_3]$ 2D building blocks of distorted NaCl type. In this last block the chalcogen atoms are positioned in three layers and occupy two different crystallographic sites (one site on the side of the block and one site in the center of the block). Tin atoms are surrounded by four chalcogen atoms forming a distorted tetrahedral environment with three different Sn−X distances as shown

**Table 4.** Atomic Coordinates and Equivalent Isotropic Displacement Parameters (Å$^2$) for $Ba_2F_2SnS_3$, $Ba_2F_2SnSe_3$, $Sr_2F_2SnSe_3$, and $Sr_2F_2SnS_3$

| atom | x | y | z | $U_{iso}$ |
|---|---|---|---|---|
| | | $Ba_2F_2SnSe_3$ | | |
| Ba | 0.7541(5) | 0.0726(1) | 0.5037(5) | 0.0085(5) |
| Sn | 0.1412(5) | 1/4 | 0.5872(5) | 0.0170(10) |
| Se1 | −0.2531(11) | 1/4 | 0.5184(10) | 0.0167(16) |
| Se2 | 0.2610(8) | 0.1356(1) | 0.4863(8) | 0.0156(10) |
| F | 0.498(4) | 0.0009(12) | 0.256(3) | 0.012(4) |
| | | $Sr_2F_2SnSe_3$ | | |
| Sr | 0.7551(8) | 0.0695(1) | 0.5029(10) | 0.0083(13) |
| Sn | 0.1492(10) | 1/4 | 0.5764(9) | 0.028(2) |
| Se1 | −0.2638(14) | 1/4 | 0.5023(15) | 0.017(2) |
| Se2 | 0.2525(11) | 0.1313(1) | 0.4930(11) | 0.0127(13) |
| F | 0.494(6) | 0.0003(16) | 0.254(5) | 0.007(5) |
| | | $Ba_2F_2SnS_3$ | | |
| Ba | 0.7520(11) | 0.0776(2) | 0.4998(11) | 0.0001(7) |
| Sn | 0.1580(11) | 1/4 | 0.5785(11) | 0.036(3) |
| S1 | −0.243(5) | 1/4 | 0.530(4) | 0.001(6) |
| S2 | 0.244(3) | 0.1388(6) | 0.519(3) | 0.004(3) |
| F | 0.498(7) | −0.005(3) | 0.256(7) | 0.012(7) |
| | | $Sr_2F_2SnS_3$ | | |
| Sr | 0.753(2) | 0.0736(3) | 0.498(2) | 0.006(2) |
| Sn | 0.165(2) | 1/4 | 0.553(2) | 0.057(4) |
| S1 | −0.245(5) | 1/4 | 0.499(7) | 0.001(7) |
| S2 | 0.246(4) | 0.1338(7) | 0.506(5) | 0.001(4) |
| F | 0.473(11) | −0.003(4) | 0.232(7) | 0.015(11) |

in Figure 3 for $Ba_2F_2SnSe_3$ (a), $Ba_2F_2SnS_3$ (b), $Sr_2F_2SnSe_3$ (c), and $Sr_2F_2SnS_3$ (d). For $Ba_2F_2SnS_3$ we could estimate the distortion of the tetrahedral site to be $d = 3.6 \times 10^{-3}$ by using the formula $d = 1/n\sum[(R - \langle R\rangle)/\langle R\rangle^2]$ with $n$ being the number of Sn−S bonds and $R$ the bond distances.[17] In most tin sulfides or selenides reported in the literature tin(IV) adopts a distorted tetrahedral or octahedral coordination. However, the distortion of the Sn site is much smaller and

(17) Shannon, R. D. *Acta Crystallogr.* **1976**, *A32*, 751.

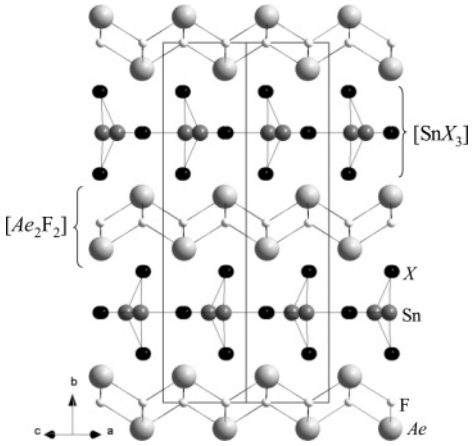


**Figure 2.** Structure of $Ba_2F_2SnSe_3$: open circles for Ba; dark gray for F; light gray for Sn; black for Se.

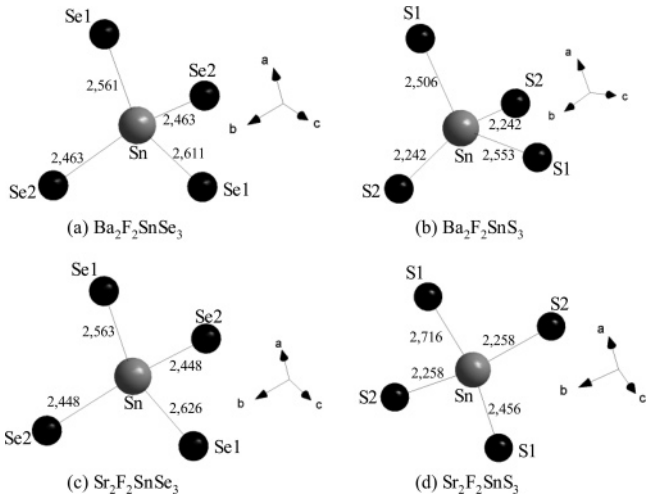


**Figure 3.** Representation of the tetrahedral coordination around the tin atoms in $Ba_2F_2SnSe_3$ (a), $Ba_2F_2SnS_3$ (b), $Sr_2F_2SnSe_3$ (c), and $Sr_2F_2SnS_3$ (d).

for example in $Ba_2SnS_4$[18] the distortion of the tetrahedral site is weak with $d$ close to $2 \times 10^{-4}$. The strongly distorted tetrahedral environment found in our compounds is rather unusual and to confirm this peculiar coordination for Sn we have performed a Mössbauer study for the pure samples of $Ba_2F_2SnSe_3$, $Sr_2F_2SnSe_3$, and $Ba_2F_2SnS_3$.

The 300 K Mössbauer spectra of the three studied compounds are quadrupole doublets (see Figure 4). The Mössbauer lines of all the spectra are as narrow as those of standard samples (e.g., $CaSnO_3$, for which $\Gamma$ = fwhm = 0.80 mm/s) used for calibration of the spectrometer, which denotes an excellent crystalline organization. For $Ba_2F_2SnS_3$ and $Sr_2F_2SnSe_3$, a shoulder can be detected in the vicinity of $v$ = 0 mm/s, which indicates the presence of an impurity containing Sn(IV) likely in oxygen surroundings. The corresponding isomer shift ($\delta$) and quadrupole splitting ($\Delta$) cannot be meaningfully refined because the contribution of this component to the total absorption area is very weak. Similar contribution cannot be detected in the spectra of $Ba_2F_2SnSe_3$.

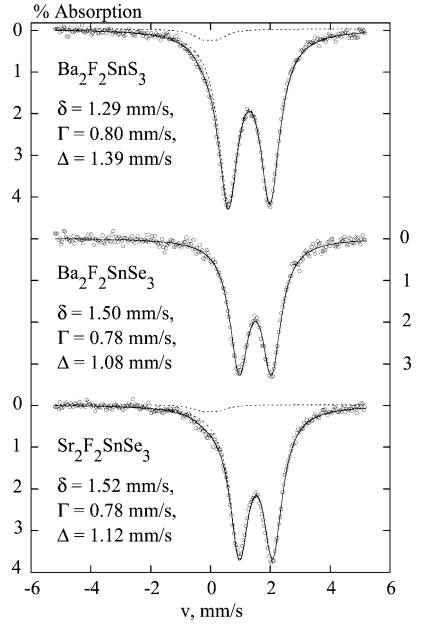


**Figure 4.** Room-temperature Mössbauer spectra recorded for $Ba_2F_2SnS_3$, $Ba_2F_2SnSe_3$, and $Sr_2F_2SnSe_3$.

**Table 5.** Mössbauer Parameters Obtained for $Ba_2F_2SnS_3$, $Ba_2F_2SnSe_3$, and $Sr_2F_2SnSe_3$[a]

| compound | $\delta$ (mm/s) ± 0.01 | $\Delta$ (mm/s) ± 0.01 | $\Gamma$ (mm/s) ± 0.01 | $\Theta_M$ (K) ± 4 |
|---|---|---|---|---|
| $Ba_2F_2SnS_3$ | 1.29 | 1.39 | 0.80 | 215 |
| $Ba_2F_2SnSe_3$ | 1.50 | 1.08 | 0.78 | 202 |
| $Sr_2F_2SnSe_3$ | 1.52 | 1.12 | 0.78 | 215 |

[a] The isomer shift ($\delta$), quadrupole splitting ($\Delta$), and line width values (fwhm = $\Gamma$) correspond to the room-temperature spectra.

The room-temperature Mössbauer parameters refined for our three compounds are given in Table 5. Values of the isomer shift clearly indicate that Fluor atoms do not surround Sn atoms and suggest Sn at the +4 oxidation state surrounded by chalcogen in agreement with the crystallographic data. The isomer shifts of our sulfide and selenide compounds are somewhat greater than those of the respective $SnS_2$ and $SnSe_2$ references (1.02−1.07 mm/s for $SnS_2$,[19,20] 1.34 mm/s for $SnSe_2$[19]). But this difference is not surprising since covalency can be anticipated to be stronger in our compounds, for two reasons. First, their structural studies evidence distorted tetrahedral coordination for tin atoms, instead of octahedral coordination in both references. Second, the presence of electropositive alkaline earth countercations, whose electrons are transferred to the anion more easily than those of tin, still amplifies the covalency of the Sn−S or Sn−Se bonds.

In most cases, Sn(IV) Mössbauer spectra are singlets, which indicates that, if present, quadrupole splitting is very weak.[21] This is not the case for our compounds (Table 5). Their important quadrupole splittings are consistent with the significant distortion of the anionic environment of tin as evidenced by the crystallographical results.

(18) Jumas, J. C.; Philippot, E.; Vermot-Gaud-Daniel, F.; Ribes, M.; Maurin, M. *J. Solid State Chem.* **1975**, *14*, 319.
(19) Pérez Vicente, C.; Tirado, J. L.; Lippens, P. E.; Jumas, J. C. *Phys. Rev. B* **1997**, *56* (11), 56.
(20) Colombet, P. Thesis, Nantes, France, 1982.
(21) Greenwood, N. N.; Gibb, T. C. *Mössbauer Spectroscopy*; Chapman and Hall: London, 1971; p 391.

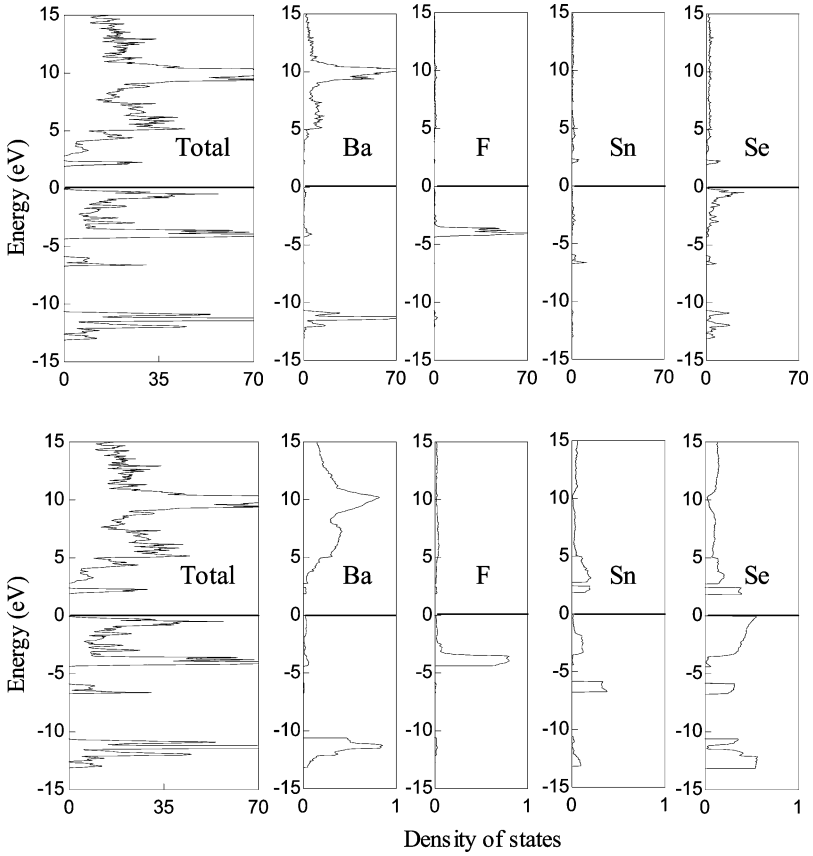


**Figure 5.** Total density of states (DOS in states per eV per cell) calculated for $Ba_2F_2SnSe_3$ (left). Partial atomic DOS represented for each atom (top right) and ratio of the partial atomic DOS to the total DOS (bottom right).

Recently, we proposed that the 2D building blocks could keep not only their structural features but also their electronic structures when assembled together to form various compounds.[5] To verify this behavior, we have undertaken band structure calculations for $BaFSnSe_3$. Figure 5 shows the total density of states that we could obtain for this compound using the LAPW method as implemented in the WIEN2K program. In this figure the projections of the density of states on each atom are also drawn. We find the Se 4p extending from −7 eV to the Fermi level. The Fluor 2p bands are located between −4.2 and −3.5 eV. A small hybridization of the F 2p states with the Ba 5d states is observed. The Ba 5p states and the Se 4s states are located around −11.3 eV. The first states found at the bottom of the conduction band are the Sn 5s, hybridized with the Se 5p, around +2.2 eV. The conduction band is mainly of Ba 5d character, and the Ba 4f states are located around +9.8 eV.

Finally, an energy gap of about 2 eV is found at the Fermi level.

We have also calculated separately the band structures of the hypothetical isolated $[Ba_2F_2]$ and $[SnSe_3]$ 2D building blocks, but with the same geometry for each as in the $Ba_2F_2SnSe_3$ compound. The resulting DOS diagrams are shown in Figure 6a,d. We have then made a comparison with the partial DOS shown in Figure 6b,c of the two building blocks calculated from the complete structure. The most significant difference is the shift of the $[Ba_2F_2]$ and $[SnSe_3]$ DOS toward higher and lower energies, respectively, when both blocks

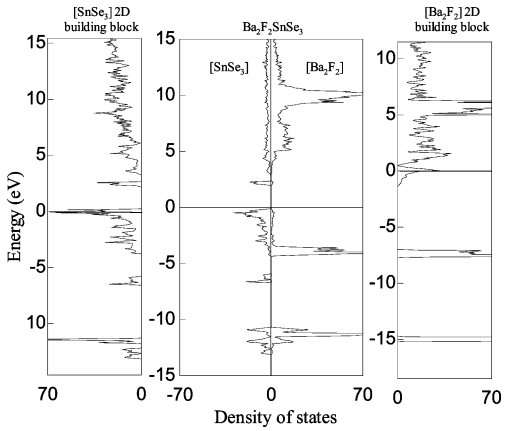


**Figure 6.** Comparison of the DOS (states per eV per cell) of the $[SnSe_3]$ and $[Ba_2F_2]$ 2D building blocks calculated as isolated entities (left and right) and projected from the total DOS of $Ba_2F_2SnSe_3$ (center).

are present. The $[Ba_2F_2]$ block alone would be metallic with an excess electron in the 5d bands. On the other hand, the $[SnSe_3]$ block alone would miss some electrons at the top of the Se 4p bands. Finally, even if a weak interaction between Ba and the Se atoms is present, we can in a first approximation describe the electronic structure of the $Ba_2F_2SnSe_3$ compound as a superposition of the band structures of the $[Ba_2F_2]$ and $[SnSe_3]$ building blocks, stabilized by the charge transfer. Consequently, the cohesion of the blocks in this compound is mainly due to ionic interactions between the charge donor $[Ba_2F_2]$ and the charge acceptor $[SnSe_3]$.

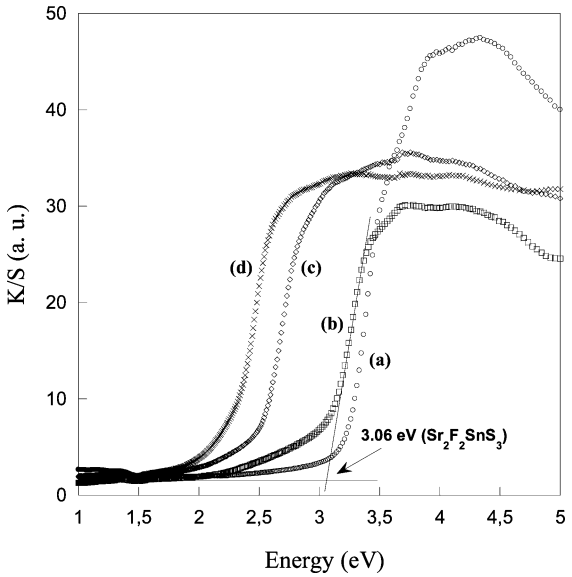


**Figure 7.** Diffuse reflectance spectra of $Ba_2F_2SnS_3$ (a), $Sr_2F_2SnS_3$ (b), $Ba_2F_2SnSe_3$ (c), and $Sr_2F_2SnSe_3$ (d) obtained after a Kubelka−Munk transformation at room temperature.

The calculated energy gap of 2 eV seems too small regarding the observed transparency of our compounds. It is well-known that GGA calculations produce smaller gaps than the experimental gap. To determine the experimental gaps of our compounds, a Kubelka−Munk transformation[22] was performed on the optical reflectivity data measured for all compounds (Figure 7). The crossing point between the baseline along the energy axis and the extrapolated line of the absorption edge gives the optical gap. The optical gaps are respectively 2.24, 2.49, 3.06, and 3.21 eV for $Sr_2F_2SnSe_3$, $Ba_2F_2SnSe_3$, $Sr_2F_2SnS_3$, and $Ba_2F_2SnS_3$. These measurements show that the gap increases from selenium to sulfur for the same alkaline earth and increases from strontium to barium for the same chalcogen. As expected, the optical gap is all the higher we used for the most electropositive metal and the most electronegative chalcogen.

$Sr_2F_2SnS_3$ and $Ba_2F_2SnS_3$ both have large optical gaps greater than 3 eV that make them transparent. This is particularly interesting as some tin compounds are known to be good n-type transparent conductors and are used in industry, as for example the fluorine-doped $SnO_2$. In that respect, $Ba_2F_2SnS_3$ could be a good candidate since it is a transparent compound. Moreover, the band structure revealed some Sn states located at the bottom of the conduction band that could allow an insulator-to-metal transition upon chemical n-type doping. This urges us to try doping the $Ba_2F_2SnS_3$ compound by substituting 10% of $Ba^{2+}$ by $La^{3+}$. Subsequently, we measured the resistivity of pressed pellets of the pure and n-doped compounds. Unfortunately, the resistance of the samples was in both cases higher than the maximal ability of our devices ($\rho > 10^9$ Ω.cm). This observation is in agreement with the band structure of $Ba_2F_2SnS_3$, which suggests insulating behavior. But it indicates that our attempt of doping was quite unsuccessful and that $Ba_2F_2SnS_3$ is not a good candidate as a transparent conductor.

## Conclusions

In conclusion, the new family of inorganic compounds $Ae_2F_2SnX_3$ (Ae = Ba, Sr; X = S, Se) could be successfully designed using fluorite and NaCl 2D building blocks. Recently, we were also able to design compounds with antifluorite[5,6] and perovskite[7] 2D building blocks. We thus believe that this concept will help solid-state chemists to design a large variety of new compounds. Moreover, choosing the proper combination of 2D building blocks should also allow targeting of an interesting property.

**Acknowledgment.** Benoît Corraze is thanked for his help in performing resistivity measurements.

**Supporting Information Available:** Crystallographic data in CIF format.

IC051592V

(22) Wendlandt, W. W.; Hecht, H. G. *Reflectance spectroscopy*; Intersciences: New York, 1966.